*Journal of Geophysical Research - Atmospheres*

Supporting Information for

# Aircraft-based observation of meteoric material in lower stratospheric aerosol particles between 15 and 68°N

Johannes Schneider[1], Ralf Weigel[2], Thomas Klimach[1], Antonis Dragoneas[1,2], Oliver Appel[1,2], Andreas Hünig[1,2], Sergej Molleker[1,2], Franziska Köllner[1], Hans-Christian Clemen[1], Oliver Eppers[1,2], Peter Hoppe[1], Peter Hoor[2], Christoph Mahnke[2,1], Martina Krämer[3], Christian Rolf[3], Jens-Uwe Grooß[3], Andreas Zahn[4], Florian Obersteiner[4], Fabrizio Ravegnani[5], Alexey Ulanovsky[6], Hans Schlager[7], Monika Scheibe[7], Glenn S. Diskin[8], Joshua P. DiGangi[8], John B. Nowak[8], Martin Zöger[9], Stephan Borrmann[2,1]

[1]Particle Chemistry Department, Max Planck Institute for Chemistry, Mainz, Germany

[2]Institute for Physics of the Atmosphere, Johannes Gutenberg University, Mainz, Germany

[3]Forschungszentrum Jülich, Institute of Energy and Climate Research (IEK-7), Jülich, Germany

[4]Karlsruhe Institute of Technology (KIT), Institute for Meteorology and Climate Research, Karlsruhe, Germany

[5]Institute of Atmospheric Sciences and Climate, ISAC-CNR, Bologna, Italy

[6]Central Aerological Observatory, Pervomayskaya 3, Dolgoprudny, Russia

[7]Institute of Atmospheric Physics, German Aerospace Center (DLR) Oberpfaffenhofen, Wessling, Germany

[8]NASA Langley Research Center, MS 483, Hampton, VA, USA

[9]Flight Experiments Department, German Aerospace Center (DLR) Oberpfaffenhofen, Wessling, Germany

## Contents of this file

## Introduction

This document contains supplementary information, with the objective to give more background information on the data interpretation. It includes the clustering parameters of the single particle data evaluation and the uncertainty estimation (S1). Individual clusters of particles are displayed (S2). The data displayed in Figure 4 of the main text are shown for the individual mission in S3. Section S4 shows the $O_3$-$H_2O$ tracer-tracer plot for StratoClim 2016 which was not used in the main text. Section S5 explains in more detail the correction for "missed" particles by using the hit rate of the mass spectrometer. The calculation of the sedimentation velocity is explained in S6. An example of sampling line loss calculation is presented in S7. Section S8 shows the results of Mie calculations used to convert the calibration data to real stratospheric refractive indices. Finally, some more information on the detection of meteoric material in tropospheric particles at the Jungfraujoch is present in S9.

### S1 Clustering Parameters.

Clustering algorithm and parameters

The individual bipolar mass spectra were sorted using the fuzzy c-means algorithm [*Bezdek et al.*, 1984; *Hinz et al.*, 1999], using the software CRISP that was written at MPIC [*Klimach et al.*, 2010; *Klimach*, 2012; *Roth et al.*, 2016]. The parameters are given in Table S1. Cations were used because the meteoric material is best recognized in the cation spectrum ($Fe^+$, $Mg^+$). Preprocessing is done by taking each ion signal to the power of 0.5 to reduce the influence of the signal intensity. The mass spectra were normalized to their sum to reduce the influence of the total ion count per spectrum. Linear correlation was chosen as distance metric (defining "similarity" of the spectra): a Pearson correlation coefficient r = 1 means that two spectra are identical. The number of clusters was prescribed with 20. A set of starting cluster centers was chosen from the data set with the condition that these clusters have Pearson correlation coefficient smaller than 0.9. The fuzzifier (originally introduced as “weighting exponent” by *Bezdek* [1981] represents the fuzziness (blurring, defocusing) of the classification. "Fuzzy abort" parameter defines the stopping criterion of the algorithm, i.e. when the differences between subsequent cluster runs change by less than the chosen value, the algorithm ends.

Variation of clustering parameters

To estimate the influence of the clustering parameters and the chosen sorting algorithm on the number of particles containing meteoric material, six additional different clustering runs were conducted for each UTLS mission. The varied parameters are: number of clusters (10, 20, 30), initialization cluster difference (0.9, 0.7), fuzzyfier (1.3, 1.5), preprocessing (power = 0.5, none), and algorithm type (fuzzy c-means, k-means). Table S2 lists the different runs, the varied parameters and the resulting number of particles containing meteorological material.
Criteria for selecting a certain cluster as "containing meteoric material" were 1) high cation signals of $Fe^+$ and $Mg^+$ (additionally allowing $Na^+$, $K^+$, $Al^+$), 2) anion signal at $HSO_4^-$, 3) vertical

profile showing increasing fractional abundance with increasing altitude, potential temperature, or potential vorticity.
In general, the standard deviation is below 6% of the mean value, and the chosen final clustering result using the parameters given in Table S1 (printed in bold) is very close to the mean value.

**S2 Individual cluster properties.**

Figures S1 through S5 show the particle clusters identified as "containing meteoric material" for the five UTLS aircraft missions.

**S3 Theta-latitude histograms for individual aircraft missions.**

Figure S6 shows the theta-latitude histograms for the five UTLS aircraft mission. All data were merged to produce Figure 4 of the main text.

**S4 Tracer-tracer correlation for StratoClim 2016.**

The $O_3$ and $H_2O$ measurements during StratoClim 2016 did not cover the whole flight time of the three measurement flights. Thus, the data were not used in Figure 8 of the main text, but for completeness are shown here in Figure S7.

**S5 ALABAMA hit rate in stratosphere and troposphere.**

In section 3.5 of the main text we calculate the absolute number concentrations of particle containing meteoric material. For this, we use the hit rate of the mass spectrometer to estimate the number of "missed" particles. Figure S8 shows the relationship between hit rate and $O_3$ which allows for estimating the contribution of "invisible" pure $H_2SO_4$ particle in the stratosphere.

**S6 Particle sedimentation in the lower stratosphere.**

The time scale for particle sedimentation was calculated as follows:
Pressure, temperature and viscosity of air were taken from the US Standard Atmosphere, using 100 m vertical resolution.
Mean free path ($\lambda$), Knudsen number ($Kn$), Cunningham correction ($C_C$) and terminal settling velocity ($V_{TS}$) were calculated using the following equations ([*Hinds*, 1999; *Seinfeld and Pandis*, 2006]):

$\lambda = \frac{1}{\sqrt{2}\pi d_m^2 N}$, with $d_m$ = collision diameter of air molecules ($3.7\times10^{-10}$ m), $N$ = number density of air molecules

$Kn = \frac{2\lambda}{d}$ with $d$ = particle diameter

$C_C = 1 + Kn\left(\alpha + \beta e^{-\frac{\gamma}{Kn}}\right)$, with $\alpha = 1.155$, $\beta = 0.471$, $\gamma = 0.596$ (Allan and Raabe, 1982)

$V_{TS} = \frac{\varrho\, d^2\, g\, C_C}{18\, \eta}$, with $\varrho$ = particle density, $g$ = acceleration of gravity, $\eta$ = viscosity of air.

The terminal settling velocity was calculated for pure $H_2SO_4$ particles ($\rho$ = 1.83 g cm$^{-3}$) and pure olivine particles ($\rho$ = 3.30 g cm$^{-3}$), assuming spherical particle shape. Figure S9 shows the terminal settling velocity as a function of altitude.

**S7 Sampling line transmission efficiency.**

The sampling line transmission efficiency was calculated here as an example for the configuration of ML-CIRRUS (ALABAMA operated on the HALO aircraft). The ¼" stainless steel sampling line that connected the HALO aerosol submicrometer inlet (HASI, *Wendisch et al.* [2016]; *Andreae et al.* [2018]) line had a total length of 2.9 m with several bends, horizontal and vertical sections. The calculations were done with a modified version of the Particle Loss Calculator (PLC) that was originally described in *von der Weiden et al.* [2009]. The modified version allows for including the sampling line pressure. The results are shown in Figure S10.

**S8 Mie calculations for stratospheric aerosol for the optical particle spectrometers OPC 1.129 and UHSAS.**

The response of the optical particle spectrometers OPC 1.129 and UHSAS for stratospheric aerosol particles was calculated using an in-house written software [*Vetter*, 2004] following the algorithms described in *Bohren and Huffmann* [1983]. The OPC 1.129 uses a laser wavelength of 655 nm. The scattered light is collected under 90° with an angular range of 60° (i.e. 60° – 120°). The UHSAS uses a laser wavelength of 1054 nm and collects the scattered light in an angular range between 22° and 158°. The refractive index for PSL, $m$ = 1.59, was taken from *Heim et al.* [2008]. The refractive index range ($m$ = 1.43 – 1.45) for lower stratospheric aerosol was taken from *Yue et al.* [1994].
The results (Figure S11) show that the lower size cut off of the OPC shifts from 250 nm to about 285 nm. For the UHSAS, the size channel with lower cut-off of 180 nm (calibrated by PSL) corresponds to 200 nm for stratospheric aerosol particles.

**S9 Jungfraujoch backtrajectories, ozone mixing ratio, and meteoric particle fraction.**

We inspected backtrajectories to obtain more information on the origin of the meteoric particles detected during the INUIT-2017 campaign at the Jungfraujoch station (3600 m altitude). For this, HYSPLIT [*Stein et al.*, 2015] back trajectories were calculated for 120 – 143 hours using the GDAS 0.5 degree data set. We chose 3600 m a.s.l. as a starting point. 27 trajectories were started per hour, using the trajectory ensemble option. All trajectory data points were binned in altitude and latitude bins and the number of trajectory points per grid is plotted in Figure S12 a) and b). Panel c) of Figure S12 shows the time series of the fraction of meteoric particles detected along with the $O_3$ mixing ratio. The fraction of meteoric particles is found to be highest between the 18$^{th}$ and 21$^{st}$ of February, a period during which the air mass

spent more time at higher altitudes and latitudes before arriving at the Jungfraujoch. A similar but less pronounced feature is found between 15$^{th}$ and 17$^{th}$ of February. These findings support the conclusion that the origin of this particle type is at higher altitudes. The dependence on latitude can be explained by the fact that mixing between stratosphere and troposphere is stronger at mid-latitudes (see Figure 8 in the main part) than in the tropics. Thus, we would expect to see a higher meteoric particle fraction when the air masses have experienced higher latitudes and altitudes, which is confirmed by Figure S12. Furthermore, a stratospheric origin is supported by the ozone trend in Panel c). The time trend of the meteoric particles follows closely the ozone time series, and even small-scale features (e.g. Feb. 09, Feb. 11, Feb. 16, and Feb. 22) are clearly visible in both time series.

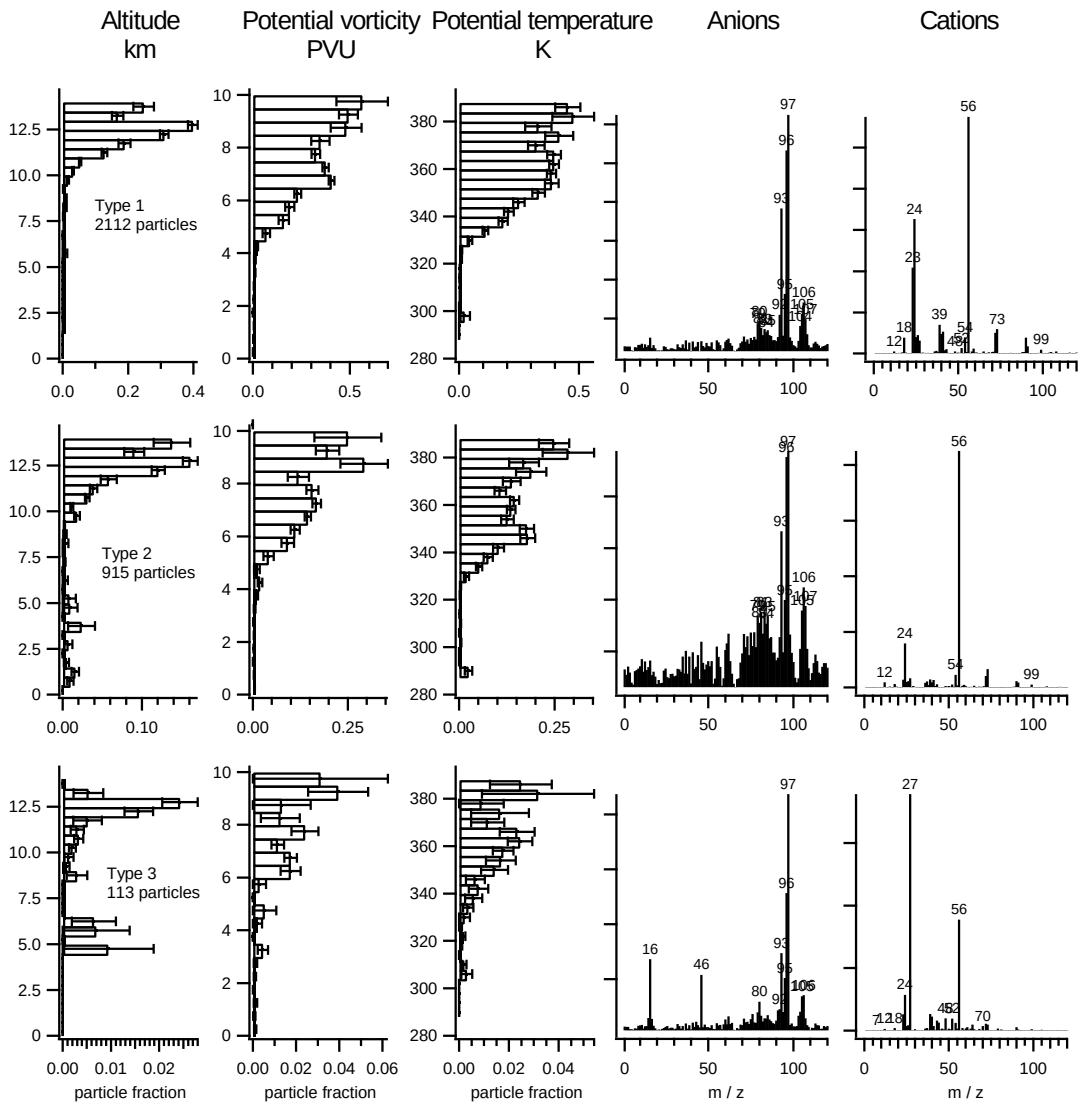


**Figure S1.** Vertical profiles and mean mass spectra of all clusters from the ML-CIRRUS 2014 data set interpreted as particles containing meteoric material. Note that the negative mass spectra (anions) are noisy, because all anion spectra of each cluster type were averaged for this display, also those where no anion signal was obtained.

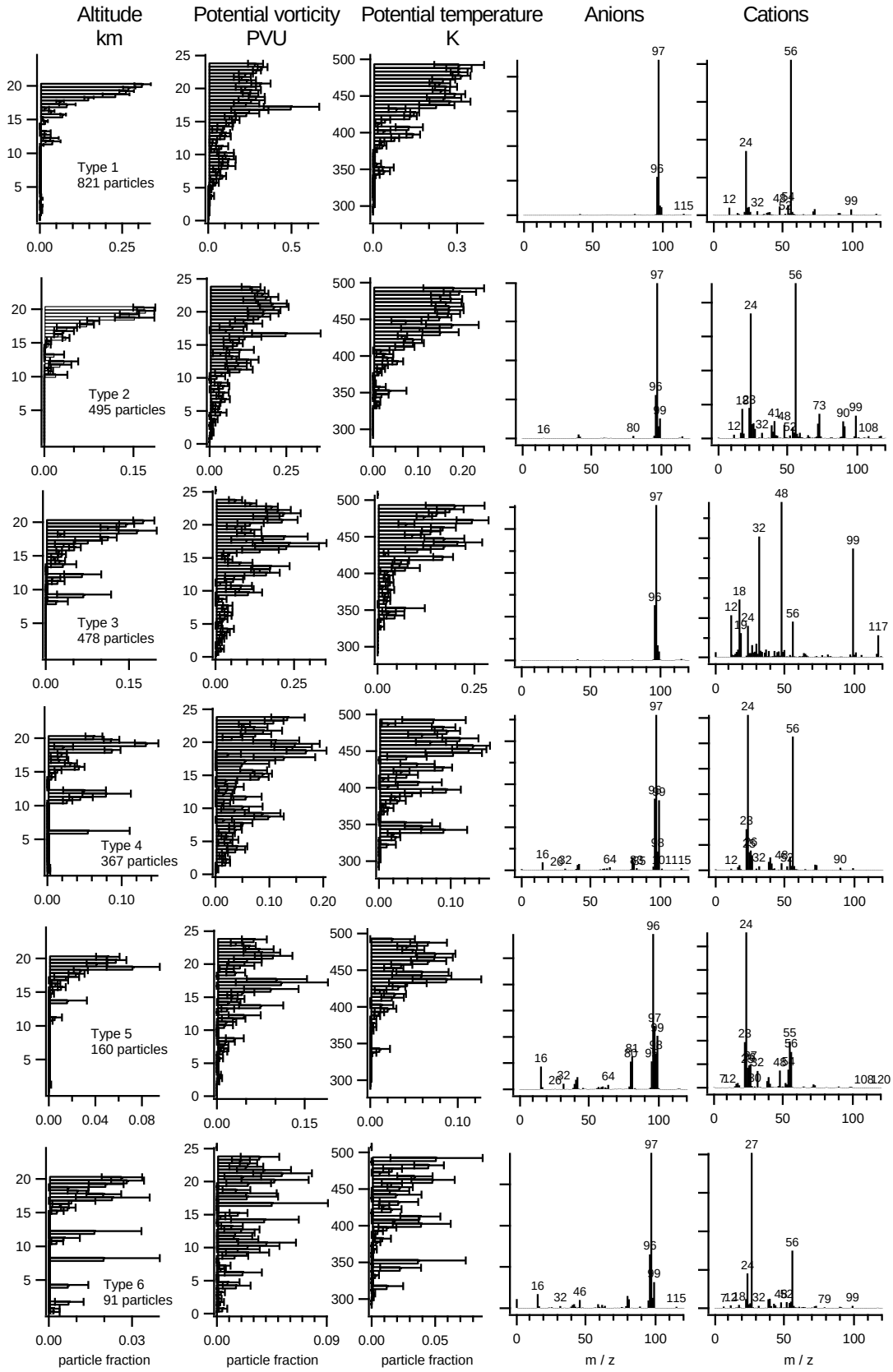
Altitude
km
Potential vorticity
PVU
Potential temperature
K
Anions
Cations
Type 1
821 particles
Type 2
495 particles
Type 3
478 particles
Type 4
367 particles
Type 5
160 particles
Type 6
91 particles
particle fraction
particle fraction
particle fraction
m / z
m / z

**Figure S2.** Vertical profiles and mean mass spectra of all clusters from the StratoClim 2016 data set interpreted as particles containing meteoric material.

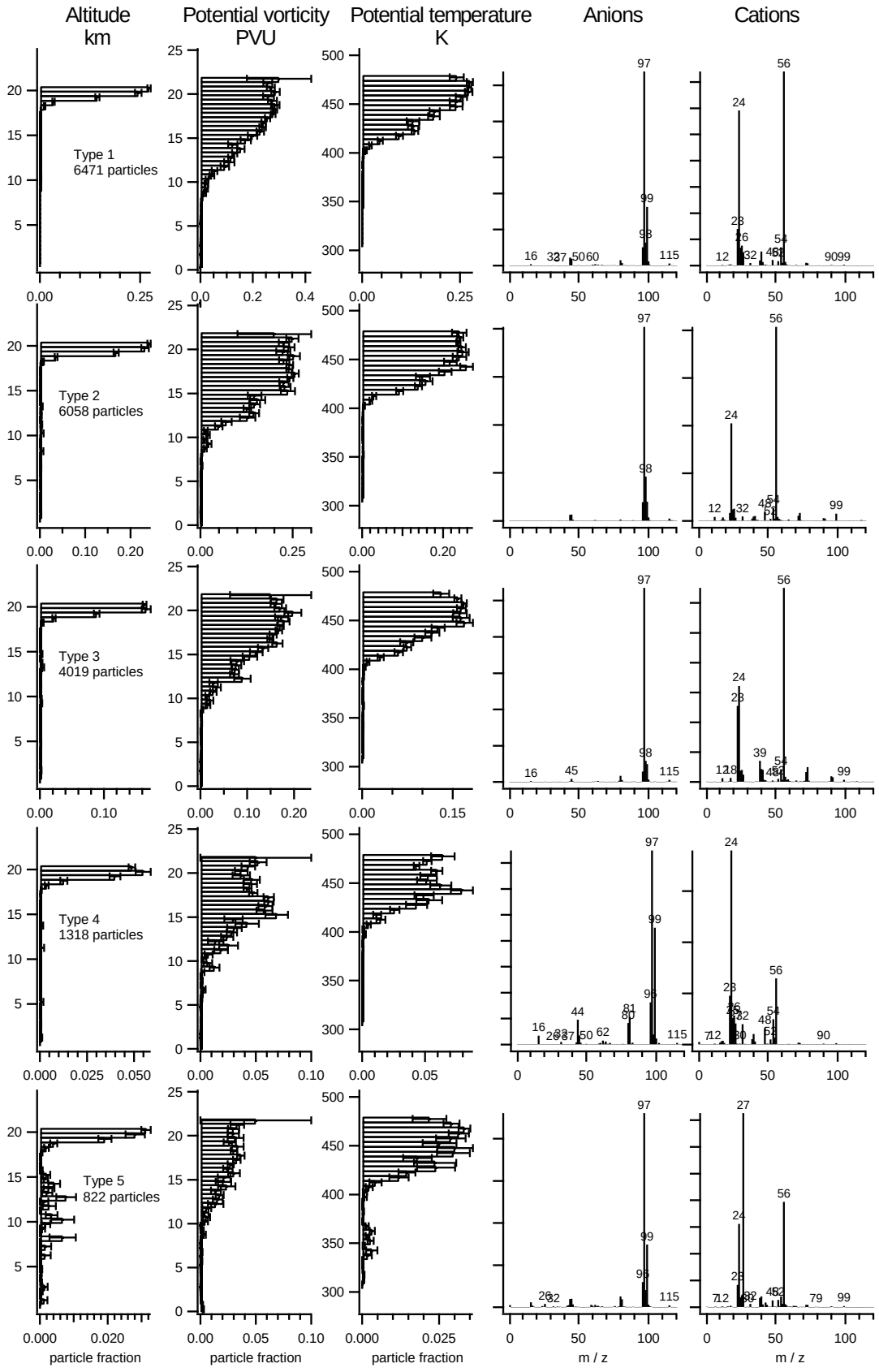
Altitude
km
Potential vorticity
PVU
Potential temperature
K
Anions
Cations
Type 1
6471 particles
Type 2
6058 particles
Type 3
4019 particles
Type 4
1318 particles
Type 5
822 particles
particle fraction
particle fraction
particle fraction
m / z
m / z

**Figure S3.** Vertical profiles and mean mass spectra of all clusters from the StratoClim 2017 data set interpreted as particles containing meteoric material.

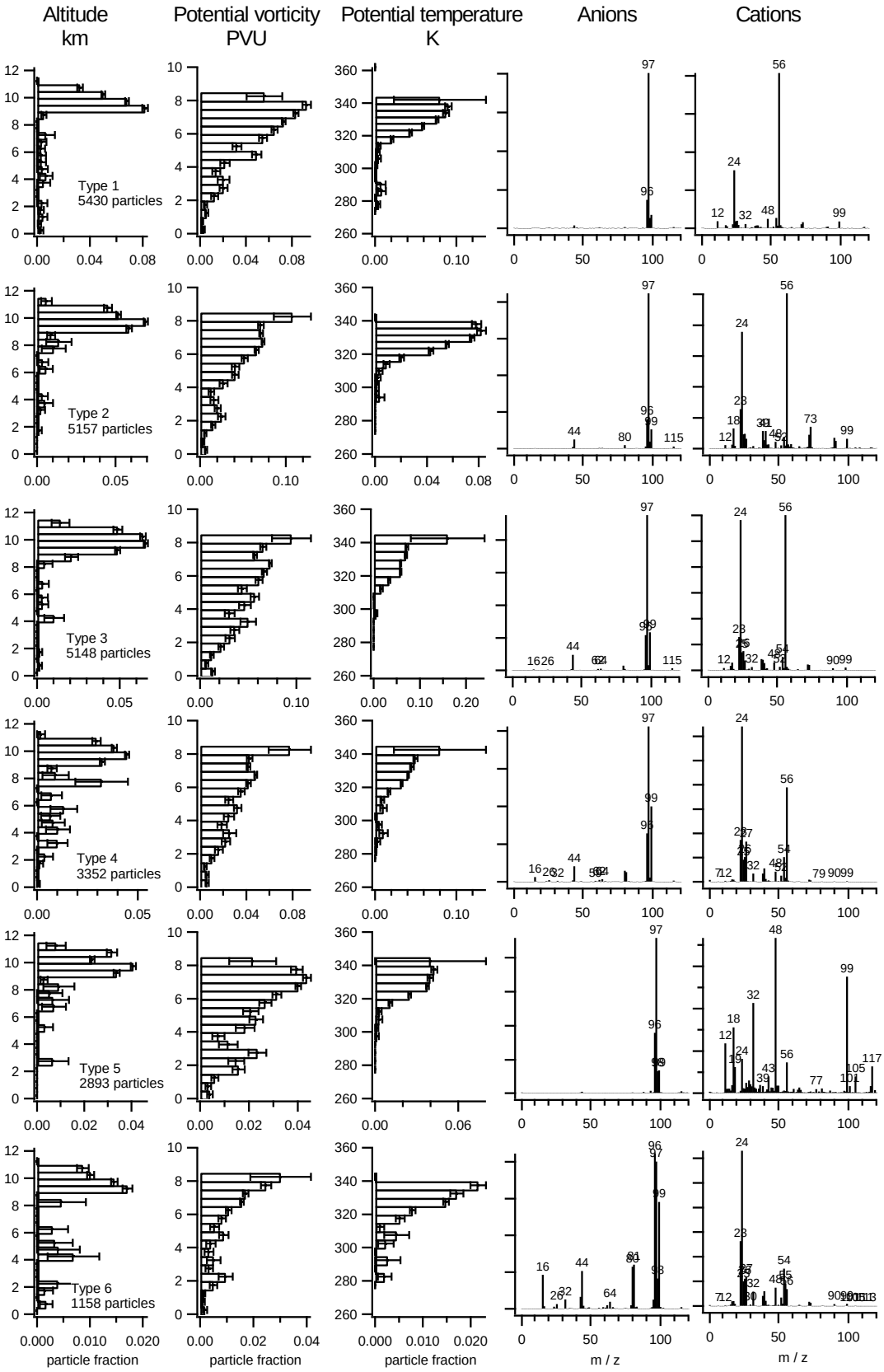
Altitude
km
Potential vorticity
PVU
Potential temperature
K
Anions
Cations
Type 1
5430 particles
Type 2
5157 particles
Type 3
5148 particles
Type 4
3352 particles
Type 5
2893 particles
Type 6
1158 particles
particle fraction
m / z

**Figure S4.** Vertical profiles and mean mass spectra of all clusters from the ND-MAX/ECLIF-2 data set interpreted as particles containing meteoric material.

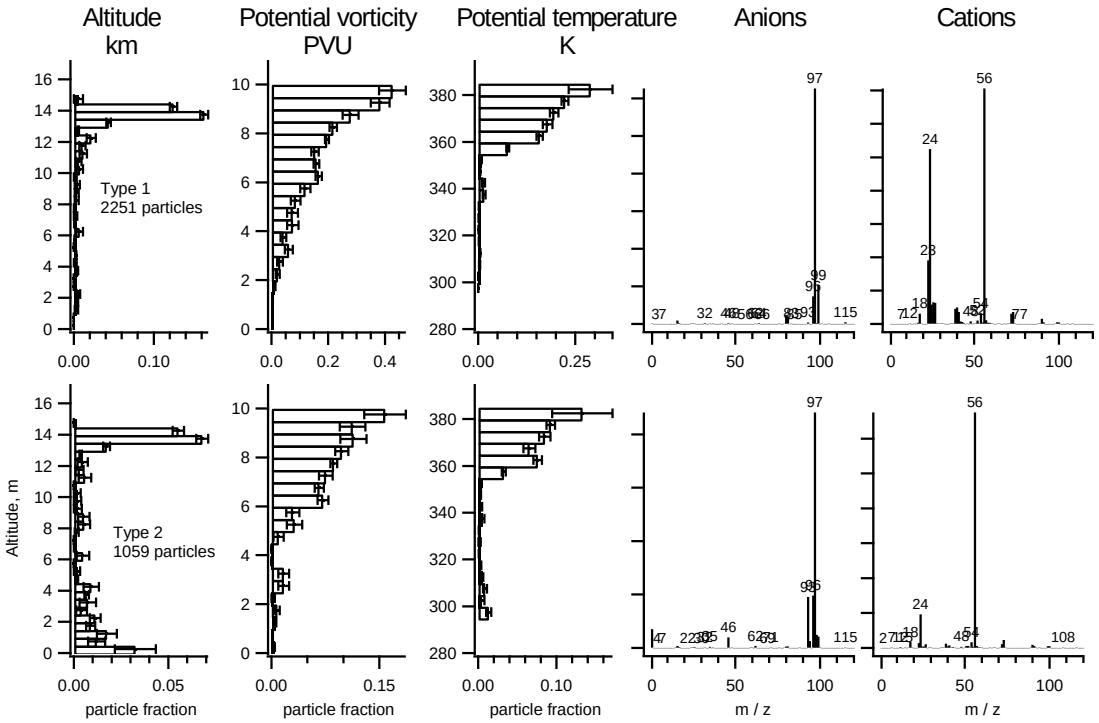


**Figure S3.** Vertical profiles and mean mass spectra of all clusters from the CAFE-Africa data set interpreted as particles containing meteoric material.

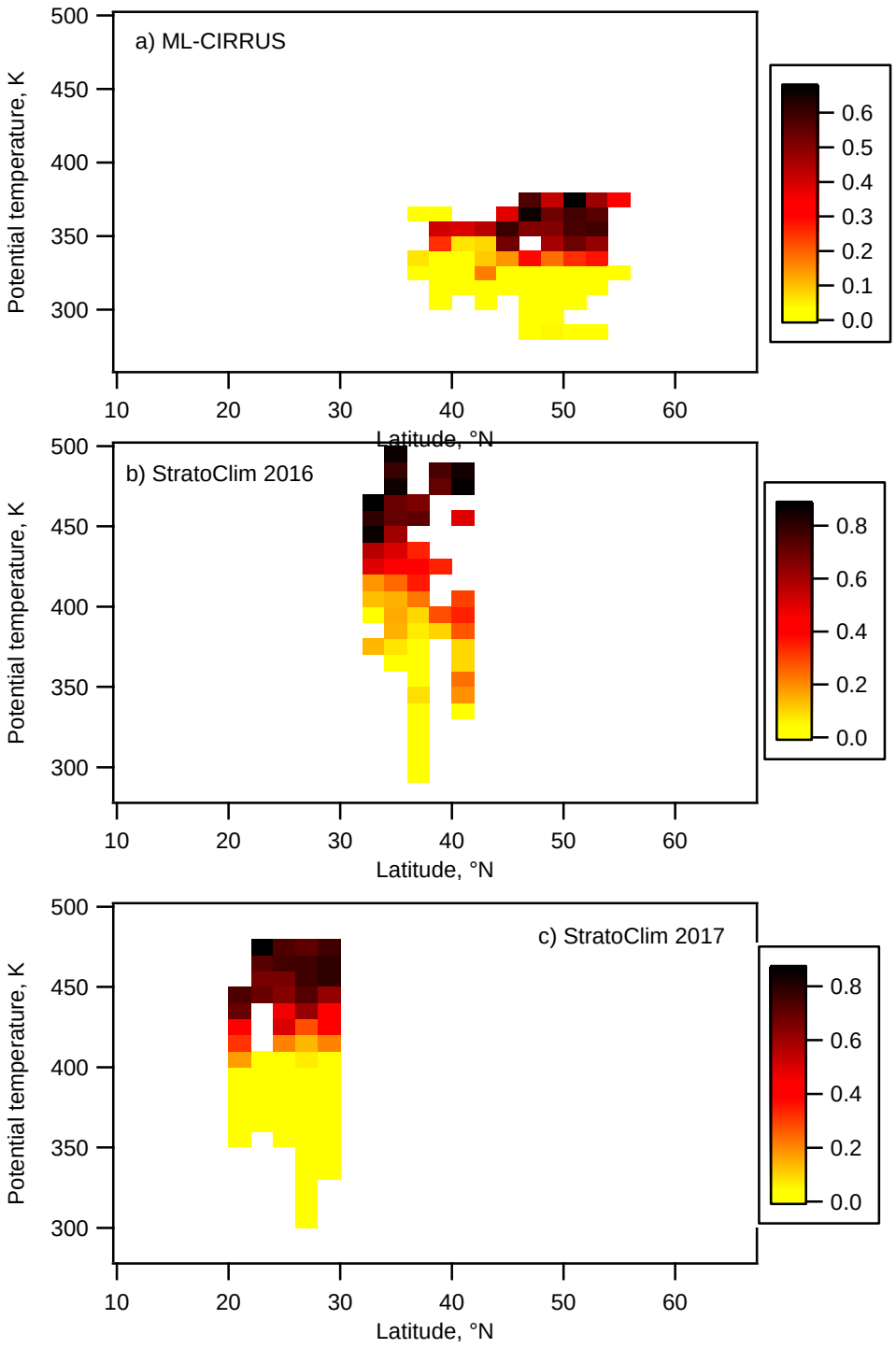
a) ML-CIRRUS
b) StratoClim 2016
c) StratoClim 2017
Potential temperature, K
Latitude, °N
500
450
400
350
300
10
20
30
40
50
60
0.6
0.5
0.4
0.3
0.2
0.1
0.0
0.8
0.6
0.4
0.2
0.0

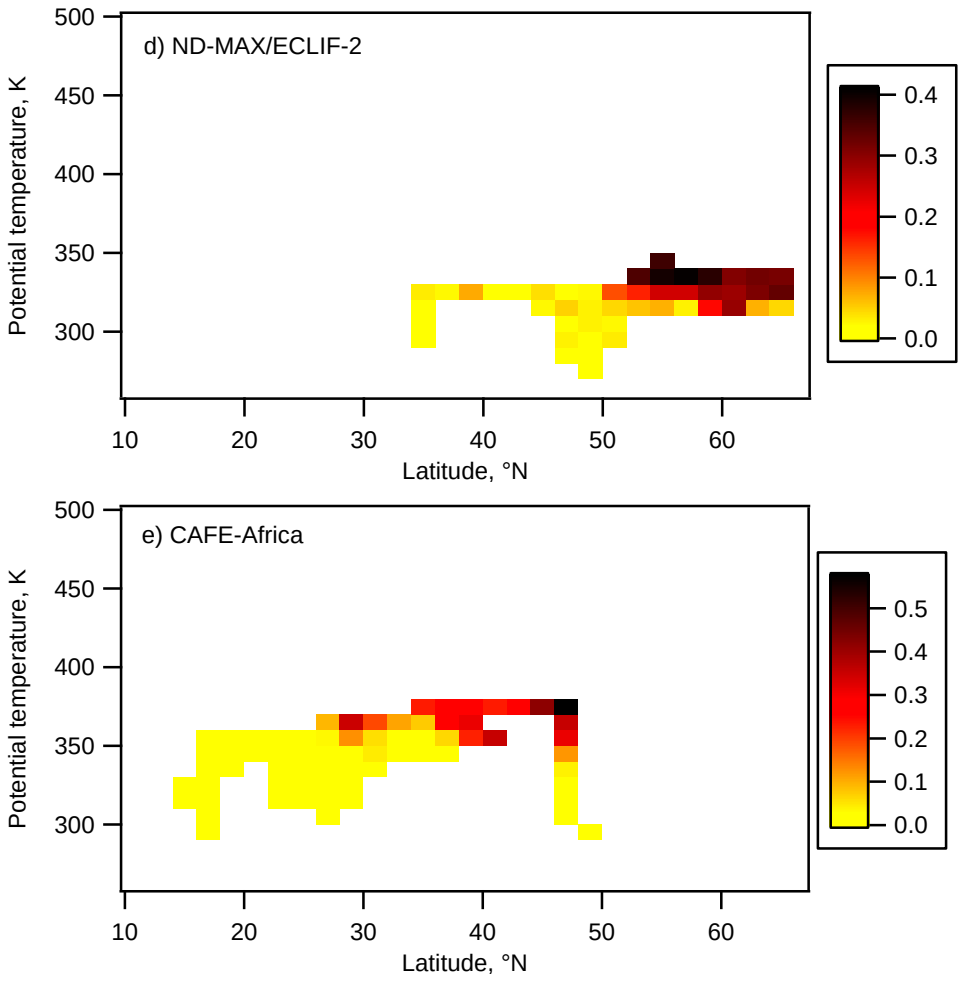


**Figure S6.** Fraction of meteoric particles as function of potential temperature and latitude for the individual missions: a) ML-CIRRUS, b) StratoClim 2016, c) StratoClim 2017, d) ND-MAX-ECLIF-2, e) CAFE-Africa.

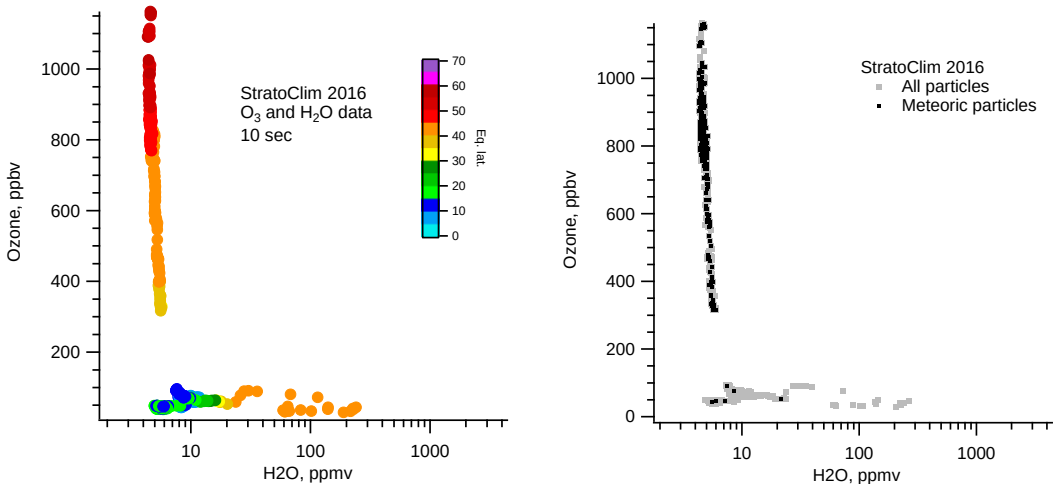


**Figure S7.** Tracer-tracer correlation for StratoClim 2016. As the instruments were not fully operative during the whole flight time of the three flights of StratoClim 2016, several gaps in the data prevent the analysis of cross-tropopause transport for this mission.

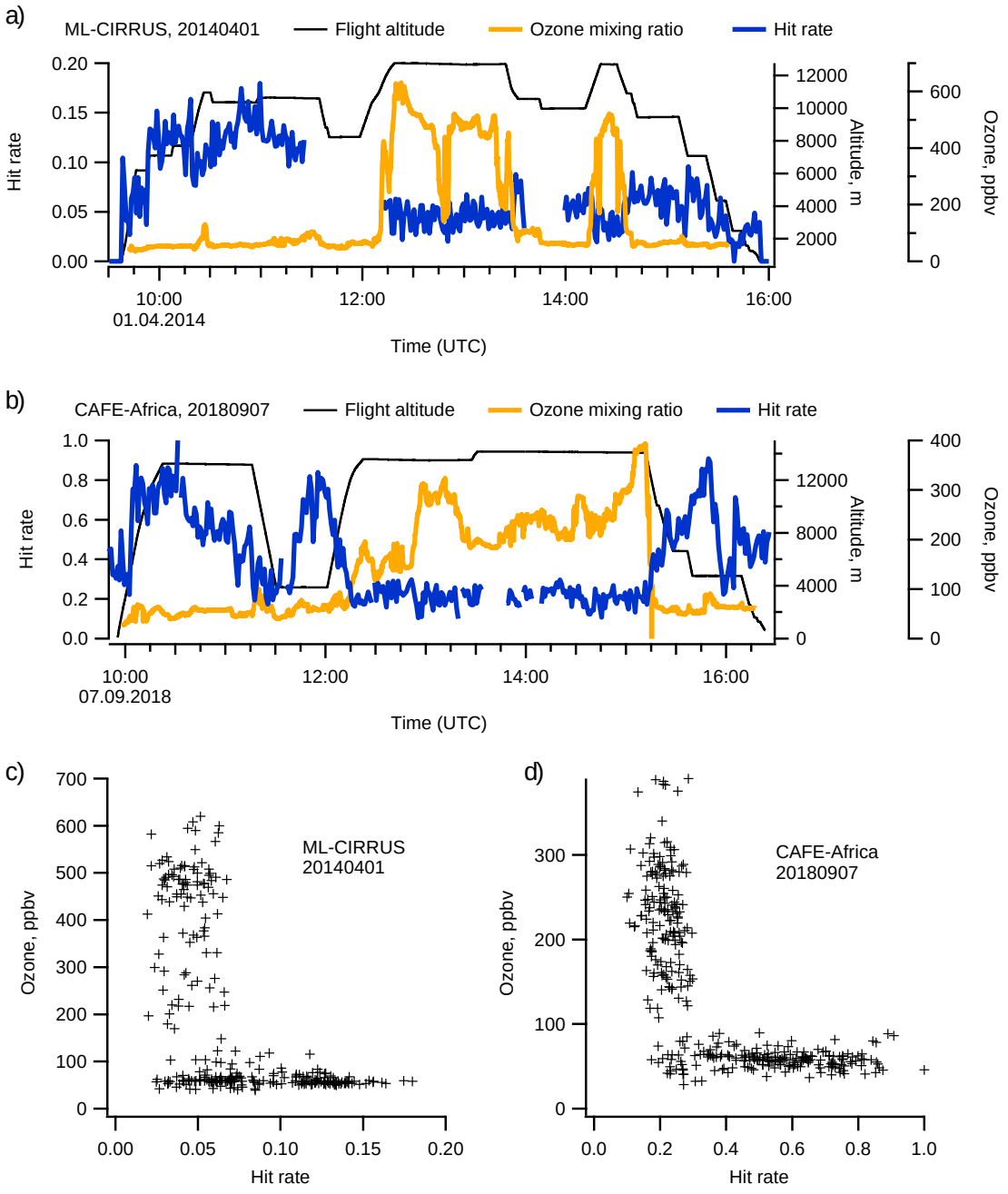


**Figure S8.** Hit rate (mass spectra per laser shot during time intervals of one minute) of ALABAMA during a) a flight on April 01, 2014 (ML-CIRRUS) and b) a flight on Sept 07, 2018 (CAFE-Africa) as a function of time along with ozone mixing ratio and flight altitude. c) + d): Hit rate versus ozone mixing ratio. Dividing between troposphere and stratosphere at 150 ppbv ozone (ML-CIRRUS) and 100 ppb ozone (CAFE-Africa), respectively, yields an average hit rate in the stratosphere of 0.044 ± 0.012 (ML-CIRRUS) and 0.21 ± 0.04 (CAFE-Africa). For the troposphere, we obtain 0.091 ± 0.037 (ML-CIRRUS) and 0.54 ± 0.18 (CAFE-Africa).

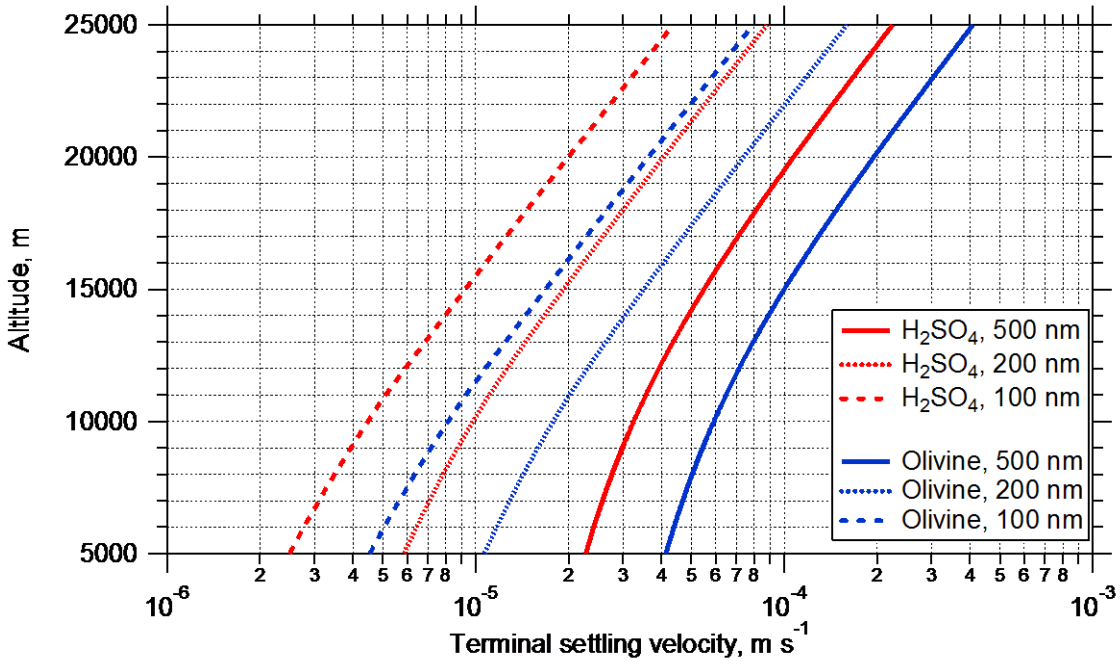


**Figure S9.** Terminal settling velocity for H2SO4 and olivine particles of 100 , 200, and 500 nm volume equivalent diameter ($d_{ve}$).

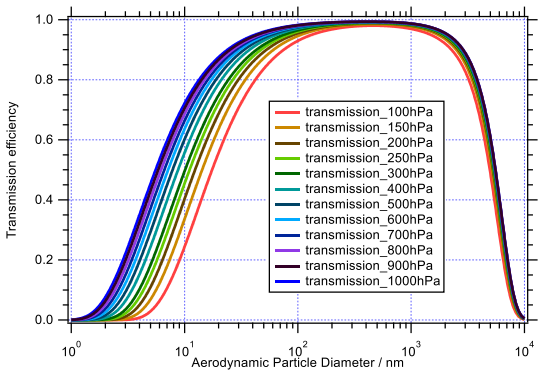


**Figure S10.** Transmission curves for the sampling line used in ML-CIRRUS that connected the HALO aerosol submicrometer inlet (HASI) to the OPC 1.129 in the ALABAMA rack.

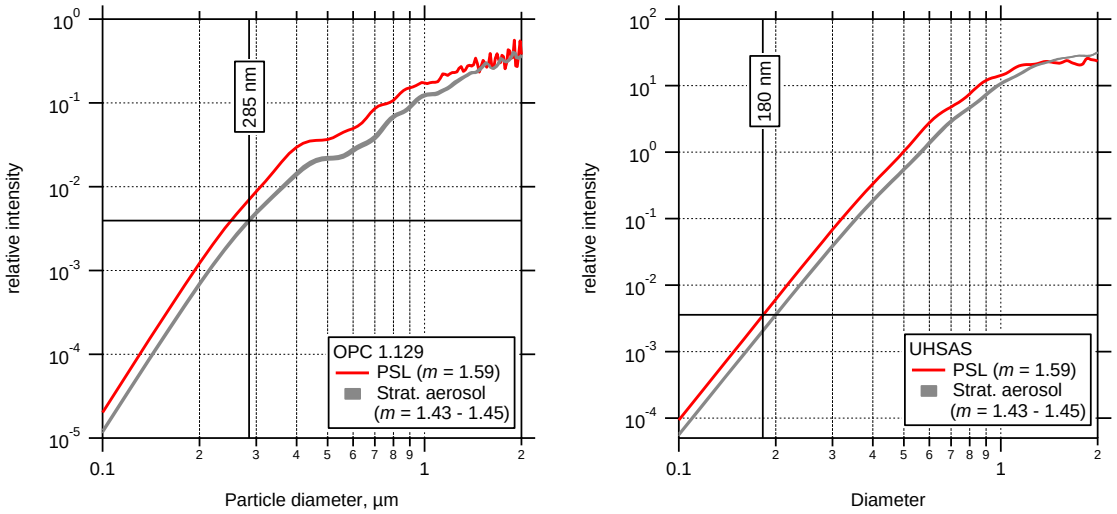


**Figure S11.** Relative intensity at the detector calculated for the OPC (Grimm 1.129, "Sky-OPC") and for the UHSAS, for PSL particles and for stratospheric particles.

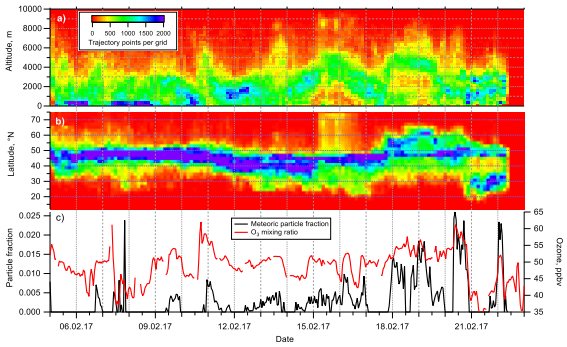


**Figure S12.** Backtrajectory information for the INUIT-JFJ 2017 field campaign at Jungfraujoch. For each hour, 27 backtrajectories were started using the trajectory ensemble option and were followed for 120 – 143 h using HYSPLIT [Stein et al., 2015] with the GADS 0.5 degree data set. Panel a) shows the number of points during which the trajectories resided in the respective altitude and time grid, Panel b) the same but for latitude. Panel c) shows the number fraction of the meteoric particles along with ozone mixing ratio.

| | |
|---|---|
| Ion type | Cations |
| Preprocessing | Power each m/z by 0.5 |
| Normalization | Sum |
| Distance metric | Correlation |
| Initialization | Different startclusters: |
| Number of clusters | 20 |
| Cluster difference | 0.9 |
| Fuzzifier | 1.3 |
| Fuzzy abort | 1e-5 |

**Table S1.** Clustering parameters used for the final analysis..

| Project | Cluster algorithm | Number of clusters | Cluster diff | Fuzzifier | Pre-processing | Number of "meteoric" particles |
|---|---|---|---|---|---|---|
| ML-CIRRUS | Fuzzy c-means | 10 | 0.9 | 1.3 | $(m/z)^{0.5}$ | 3080 |
| | **Fuzzy c-means** | **20** | **0.9** | **1.3** | **$(m/z)^{0.5}$** | **3140** |
| | Fuzzy c-means | 30 | 0.9 | 1.3 | $(m/z)^{0.5}$ | 3136 |
| | Fuzzy c-means | 20 | 0.7 | 1.3 | $(m/z)^{0.5}$ | 2931 |
| | Fuzzy c-mean | 20 | 0.9 | 1.5 | $(m/z)^{0.5}$ | 3136 |
| | Fuzzy c-means | 20 | 0.9 | 1.3 | none | 3051 |
| | k-means | 20 | 0.9 | N/A | $(m/z)^{0.5}$ | 3247 |
| Mean ± StdDev | | | | | | 3103 ± 90 |
| | | | | | | |
| StratoClim 2016 | Fuzzy c-means | 10 | 0.9 | 1.3 | $(m/z)^{0.5}$ | 2357 |
| | **Fuzzy c-means** | **20** | **0.9** | **1.3** | **$(m/z)^{0.5}$** | **2412** |
| | Fuzzy c-means | 30 | 0.9 | 1.3 | $(m/z)^{0.5}$ | 2679 |
| | Fuzzy c-means | 20 | 0.7 | 1.3 | $(m/z)^{0.5}$ | 2376 |
| | Fuzzy c-mean | 20 | 0.9 | 1.5 | $(m/z)^{0.5}$ | 2567 |
| | Fuzzy c-means | 20 | 0.9 | 1.3 | none | 2618 |
| | k-means | 20 | 0.9 | N/A | $(m/z)^{0.5}$ | 2570 |
| Mean ± StdDev | | | | | | 2511 ± 118 |
| | | | | | | |
| StratoClim 2017 | Fuzzy c-means | 10 | 0.9 | 1.3 | $(m/z)^{0.5}$ | 18355 |
| | **Fuzzy c-means** | **20** | **0.9** | **1.3** | **$(m/z)^{0.5}$** | **18688** |
| | Fuzzy c-means | 30 | 0.9 | 1.3 | $(m/z)^{0.5}$ | 19700 |
| | Fuzzy c-means | 20 | 0.7 | 1.3 | $(m/z)^{0.5}$ | 18688 |
| | Fuzzy c-mean | 20 | 0.9 | 1.5 | $(m/z)^{0.5}$ | 18459 |
| | Fuzzy c-means | 20 | 0.9 | 1.3 | none | 21235 |
| | k-means | 20 | 0.9 | N/A | $(m/z)^{0.5}$ | 20215 |
| Mean ± StdDev | | | | | | 19334 ± 1006 |
| | | | | | | |
| ND-MAX/ ECLIF-2 | Fuzzy c-means | 10 | 0.9 | 1.3 | $(m/z)^{0.5}$ | 20141 |
| | **Fuzzy c-means** | **20** | **0.9** | **1.3** | **$(m/z)^{0.5}$** | **23138** |
| | Fuzzy c-means | 30 | 0.9 | 1.3 | $(m/z)^{0.5}$ | 21883 |
| | Fuzzy c-means | 20 | 0.7 | 1.3 | $(m/z)^{0.5}$ | 21681 |
| | Fuzzy c-mean | 20 | 0.9 | 1.5 | $(m/z)^{0.5}$ | 21126 |
| | Fuzzy c-means | 20 | 0.9 | 1.3 | none | 21752 |
| | k-means | 20 | 0.9 | N/A | $(m/z)^{0.5}$ | 18998 |
| Mean ± StdDev | | | | | | 21245 ± 1237 |
| | | | | | | |
| CAFE-Africa | Fuzzy c-means | 10 | 0.9 | 1.3 | $(m/z)^{0.5}$ | 3325 |
| | **Fuzzy c-means** | **20** | **0.9** | **1.3** | **$(m/z)^{0.5}$** | **3310** |
| | Fuzzy c-means | 30 | 0.9 | 1.3 | $(m/z)^{0.5}$ | 3290 |
| | Fuzzy c-means | 20 | 0.7 | 1.3 | $(m/z)^{0.5}$ | 3194 |
| | Fuzzy c-mean | 20 | 0.9 | 1.5 | $(m/z)^{0.5}$ | 3281 |
| | Fuzzy c-means | 20 | 0.9 | 1.3 | none | 3287 |
| | k-means | 20 | 0.9 | N/A | $(m/z)^{0.5}$ | 3515 |
| Mean ± StdDev | | | | | | 3314 ± 90 |
| | | | | | | |

**Table S1.** Variations of clustering parameters. The inferred number of particles containing meteoric material is given in the last column. Other parameters were kept as in Table S1.

## References


Andreae, M. O., et al. (2018), Aerosol characteristics and particle production in the upper troposphere over the Amazon Basin, *Atmos. Chem. Phys.*, *18*(2), 921-961, doi:10.5194/acp-18-921-2018.

Bezdek, J. C. (1981), *Pattern Recognition with Fuzzy Objective Function Algorithms*, Plenum Press, New York, USA.

Bezdek, J. C., R. Ehrlich, and W. Full (1984), FCM: The fuzzy c-means clustering algorithm, *Computers & Geosciences*, *10*(2), 191-203, doi:10.1016/0098-3004(84)90020-7.

Bohren, C. F., and D. R. Huffmann (1983), *Absorption and scattering of light by small particles*, Wiley and Sons, New York.

Heim, M., B. J. Mullins, H. Umhauer, and G. Kasper (2008), Performance evaluation of three optical particle counters with an efficient "multimodal" calibration method, *J. Aerosol. Sci.*, *39*(12), 1019-1031, doi:https://doi.org/10.1016/j.jaerosci.2008.07.006.

Hinds, W. C. (1999), *Aerosol technology - properties, behaviour, and measurements of airborne particles*, 2. ed., John Wiley & Sons, Inc., New York.

Hinz, K. P., M. Greweling, F. Drews, and B. Spengler (1999), Data processing in on-line laser mass spectrometry of inorganic, organic, or biological airborne particles, *Journal of the American Society for Mass Spectrometry*, *10*(7), 648-660, doi:10.1016/s1044-0305(99)00028-8.

Klimach, T. (2012), Chemische Zusammensetzung der Aerosole: Design und Datenauswertung eines Einzelpartikel-Laserablationsmassenspektrometers, Ph.D. thesis (in German), Johannes Gutenberg-Universität, Mainz, Germany, doi:http://nbn-resolving.de/urn:nbn:de:hebis:77-33547.

Klimach, T., F. Drewnick, and S. Borrmann (2010), CRISP - a new tool for analysis of single particle mass spectra, in *International Aerosol Conference*, edited, Helsinki.

Roth, A., J. Schneider, T. Klimach, S. Mertes, D. van Pinxteren, H. Herrmann, and S. Borrmann (2016), Aerosol properties, source identification, and cloud processing in orographic clouds measured by single particle mass spectrometry on a central European mountain site during HCCT-2010, *Atmos. Chem. Phys.*, *16*(2), 505-524, doi:10.5194/acp-16-505-2016.

Seinfeld, J. H., and S. N. Pandis (2006), *Atmospheric chemistry and physics: from air pollution to climate change* John Wiley and Sons, Hoboken, NJ.

Stein, A. F., R. R. Draxler, G. D. Rolph, B. J. B. Stunder, M. D. Cohen, and F. Ngan (2015), NOAA's HYSPLIT Atmospheric Transport and Dispersion Modeling System, *Bulletin of the American Meteorological Society*, *96*(12), 2059-2077, doi:doi:10.1175/BAMS-D-14-00110.1.

Vetter, T. (2004), Berechnung der Mie-Streufunktionen zur Kalibrierung optischer Partikelzähler, *Diploma thesis (in German)*, *University Mainz*.

von der Weiden, S. L., F. Drewnick, and S. Borrmann (2009), Particle Loss Calculator – a new software tool for the assessment of the performance of aerosol inlet systems, *Atmos. Meas. Tech.*, *2*(2), 479-494, doi:10.5194/amt-2-479-2009.

Wendisch, M., et al. (2016), ACRIDICON–CHUVA Campaign: Studying Tropical Deep Convective Clouds and Precipitation over Amazonia Using the New German Research Aircraft HALO, *Bulletin of the American Meteorological Society*, *97*(10), 1885-1908, doi:10.1175/BAMS-D-14-00255.1.

Yue, G. K., L. R. Poole, P. H. Wang, and E. W. Chiou (1994), Stratospheric aerosol acidity, density, and refractive-index deduced from SAGE-II and NMC temperature data, *J. Geophys. Res.-Atmos.*, *99*(D2), 3727-3738, doi:10.1029/93jd02989.